TYPE Original Research
PUBLISHED 26 September 2025
DOI 10.3389/feart.2025.1643201



OPEN ACCESS

EDITED BY

Ramanathan Alagappan, Independent Researcher, Tiruchirapalli, India

REVIEWED BY
Douaa Fathy,
Minia University, Egypt
Alok Kumar,
Banaras Hindu University, India

*CORRESPONDENCE Jing Li,

☑ lijing@sxie.edu.cn

RECEIVED 08 June 2025 ACCEPTED 01 September 2025 PUBLISHED 26 September 2025

CITATION

Li J and Wang L (2025) Study on coal facies evolution and the coal-forming environment of the L_2 coal seam in Juhugeng mine, Muli coalfield, Qinghai province. Front. Earth Sci. 13:1643201. doi: 10.3389/feart.2025.1643201

COPYRIGHT

© 2025 Li and Wang. This is an open-access article distributed under the terms of the Creative Commons Attribution License (CC BY). The use, distribution or reproduction in other forums is permitted, provided the original author(s) and the copyright owner(s) are credited and that the original publication in this journal is cited, in accordance with accepted academic practice. No use, distribution or reproduction is permitted which does not comply with these terms.

Study on coal facies evolution and the coal-forming environment of the L₂ coal seam in Juhugeng mine, Muli coalfield, Qinghai province

Jing Li* and Lu Wang

Department of Geology and Surveying Engineering, Shanxi Institute of Energy, Jinzhong, Shanxi, China

Maceral composition in coal varies significantly under the influence of different sedimentary environments. This study applies coal petrology techniques to elucidate the controlling mechanisms of coal-forming environments on macerals, focusing on the L_2 coal seam from the Juhugeng mine in the Muli coalfield. The results reveal that the lower section of the L_2 coal seam is predominantly composed of semi-bright coal, transitioning upward into durain and semi-dull coal. Vitrinite is the dominant maceral, followed by inertinite, while clay minerals constitute the primary inorganic component. Based on vertical variations in coal facies, the L_2 coal seam is subdivided into three evolutionary stages from bottom to top: a wet forest swamp facies, a wet herbaceous swamp facies, and a return to wet forest swamp facies. These transitions reflect dynamic changes in peat-forming conditions, likely driven by subtle shifts in hydrology, vegetation input, and clastic influx.

KEYWORDS

coal facies evolution, macerals, coal-forming environment, Juhugeng mine, Muli coalfield

1 Introduction

Coal is a fundamental energy source and a critical industrial raw material in China, making its stable supply essential for national energy security (Li and Hu, 2017; Yuan, 2018). Coal facies analysis is of great significance for restoring the sediment source and sediment environment. Many scholars have established different coal facies parameters through in-depth research on macerals, coal-forming plants, and peat bogs (Harvey and Dillon, 1985; McCabe, 1987; Marchioni and Kalkreuth, 1991; Calder et al., 1991; Diessel and Diessel, 1992; Gmur and Kwiecińska, 2002; Suárez-Ruiz and Jiménez, 2004; Kalkreuth, 2004; Silva and Kalkreuth, 2005; Jiu et al., 2021; Nath and Kumar, 2022; Singh and Kumar, 2017; Singh and Kumar, 2020). Diessel (1982), Diessel (1986), Diessel (2007) introduced the gelification index (GI) and tissue preservation index (TPI) to characterize peat-bog environments and coal-forming plant categories. Calder et al. (1991) proposed the groundwater index (GWI) and vegetation index (VI) to evaluate the coal-forming vegetation type and the hydrodynamic conditions of the peat depositional environment. The vitriniteto-inertinite (V/I) ratio, as suggested by Harvey and Dillon (1985), is used as an indicator of overlying water depth and the climate type. Silva and Kalkreuth (2005) classified the peat sedimentary environment into three types based on the T-D-F diagram. Based on the

comprehensive utilization of multiple coal facies parameters, the characteristics of coal facies evolution, climate, water table, and sedimentary environment were analyzed (Dai et al., 2007; Zhang et al., 2010; Li et al., 2014; Lu et al., 2017; Zhao et al., 2017; Feng et al., 2019; Guatame and Rincón, 2021; Kumar et al., 2020; 2021; 2024), providing important insights for the clean and efficient utilization of coal resources.

The Muli coalfield hosts abundant coal resources, with the Juhugeng mine situated in its central-western region (Wang et al., 2020). As a major coal production base, the Juhugeng mine contains significant reserves primarily within the Middle Jurassic coalbearing strata (Wen et al., 2006; 2011). Previous studies in this area have primarily focused on coal-bearing strata, sequence strata, tectonic control of coal seams, coal measure gases, and geochemistry in the Juhugeng mine (Cao et al., 2009; Yang et al., 2011; Wang et al., 2017; Shang et al., 2018; Wang et al., 2020; Huo et al., 2020; Li et al., 2022). However, although many studies have focused on coal facies analysis in other regions, there is limited research on the coal facies characteristics of the Juhugeng mine in the Muli coalfield. This study aims to fill this gap by investigating the coal petrology and coal facies features of the L₂ coal seam in the Juhugeng mine. Therefore, this study takes samples from the L2 coal seam in the Juhugeng mine as the research object; the coal petrology and coal facies characteristics were analyzed, and the coal-forming environment was explored. The novelty of this study lies in its detailed analysis of the coal facies evolution in the Juhugeng mine, an area with rich coal resources but limited research on its coal facies characteristics. By focusing on this under-researched aspect, this study offers new perspectives on the coal-forming environment. The findings will contribute to a better understanding of coal facies evolution.

This study offers valuable insights into the coal facies characteristics and coal-forming environment of the $\rm L_2$ coal seam in the Juhugeng mine, contributing to improved understanding of local coal resource management and clean utilization. The application of established coal facies parameters enhances the interpretation of sedimentary conditions and peat-forming processes. However, the focus on a single seam limits the broader applicability of the results within the Muli coalfield. Future studies should incorporate multiseam comparisons and regional tectonic context to provide a more comprehensive framework for coal facies evolution.

2 Geological setting

The Muli Basin is situated on the northeast edge of the Qinghai–Tibetan Plateau, within the middle Qilian fault uplift zone of the Qilian orogenic belt (Shang et al., 2018). The Muli coalfield has experienced frequent regional tectonic movements since the Proterozoic era, and lithosphere deformation was relatively weak (Wen et al., 2011). The structural framework of the Muli coalfield was primarily established during the Paleozoic as a result of subduction between the Tsaidam and North Qilian blocks (Pan et al., 2009). The Caledonian movement during this period laid the structural framework of the uplifts and depressions within the region, and the geomorphic feature of high northeast and low southwest was formed as a whole (Ramsay and Huber, 1987).

The Juhugeng mine, located in the central and western part of the Muli coalfield (Figure 1a), lies in the western section of

the Middle Qilian Block, shaped by the Qilian tectonic movement (Wang et al., 2020). The structural line direction of the Juhugeng mine is northwest-oriented, and the tectonics is a compound syncline. The Juhugeng mine is divided into four mines and three open-pit mines (Wen et al., 2006) (Figure 1b). The Middle Jurassic coal-bearing strata form synclines on both the northern and southern flanks, while a Triassic anticline dominates the central zone, forming the core of the mine's structure. Large-scale thrust faults, trending from northwest to southeast, are well developed along the fold margins (Shao et al., 2015). Compression from south to north has caused steep inversion of strata on both synclinal limbs (Figure 1b), with more intense deformation observed in the southern part of the mine (Wen et al., 2011).

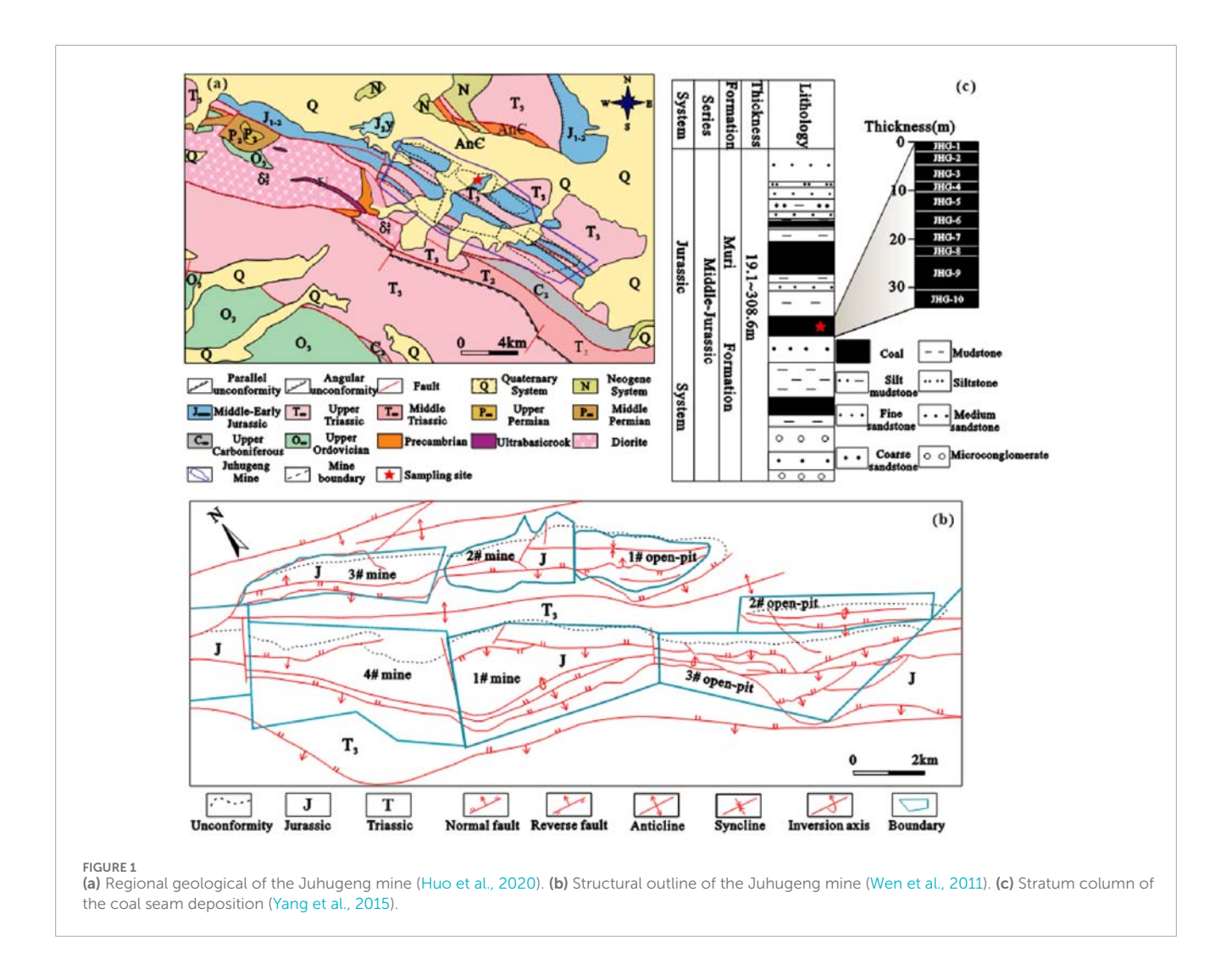
The coal-bearing strata in the Juhugeng mine belong to the Middle Jurassic Muli Formation and Jiangcang Formation (Wen et al., 2006). The lower part of the Muli Formation represents a braided-river alluvial-plain environment, characterized by the deposition of coarse clastic rocks. The upper part is mainly a delta front-lagoon deposit environment, with two thick coal seams— L_1 and L_2 . The L_2 coal seam was formed in the sedimentary environment of peat bogs formed by the siltation of braids and the expansion of lakes. During this period, the peat accumulation rate and the rate of basin subsidence were approximately balanced, resulting in the stable and widespread development of the L_2 coal seam (Shao et al., 2015).

3 Materials and methods

The collected samples are considered representative and reliable; therefore, systematic sampling was conducted at the base of the upper Muli Formation in the Juhugeng mine in accordance with (Chinese National Standard GB/T 482-2008, Standardization Administration of China, 2008). A total of 10 fresh coal samples (JHG-1 to JHG-10) were collected from fresh outcrops using hand tools (Figure 1c). The exposed coal surface was first cleaned to remove weathered material, and then fresh coal was chipped from the vertical profile at regular depth intervals. All samples were immediately sealed in airtight plastic bags and labeled to avoid contamination and oxidation before laboratory analysis.

The macroscopic type characteristics of the samples were described in accordance with (Chinese National Standard GB/T 18023-2000, Standardization Administration of China, 2008). The macroscopic types of the collected samples are semi-bright coal, durain, and semi-dull coal.

The samples were crushed to a size of less than 20 mesh for polished slices, which were used to measure the reflectivity and observe macerals and minerals under a microscope. The characteristics of coal macerals were observed and quantitatively analyzed under oil-immersed reflected light using a Leica DM4500P Optical Microscope, based on the ICCP System (International Committee for Coal and Organic Petrology, 1998, International Committee for Coal and Organic Petrology, 2001; Pickel et al., 2017), with more than 500 effective measurement point. Maceral analysis was conducted by counting 500 points for each sample. The counted points include vitrinite, inertinite, liptinite, and mineral matter. The proportions represent the relative abundance of each component as a percentage of the



total points counted, and therefore, the sum of macerals and minerals equals 100%. The random reflectance ($R_{o,ran}$) was determined using a CRAIC 20/30PV micro-spectrophotometer, in accordance with ASTM standard D2798-11A (2011). The reflectance analysis ($R_{o,ran}$) consists of 100 measurement points in vitrinite. A yttrium aluminum garnet reflectance standard (R_{oil} = 0.903%, λ = 546 nm) was used to calibrate the accuracy of the reflectance measurements, and the measurement error of the standard sample was less than 2%.

4 Results

4.1 Macroscopic type

The macroscopic types are shown in Table 1. The average $R_{\rm o,ran}$ value is 0.97%, ranging from 0.89% to 1.09%. The samples JHG-1, JHG-3, and JHG-5 are classified as durain, characterized by massive or banded structures, weak asphaltic luster, and poorly developed fractures. The samples JHG-2, JHG-4, and JHG-10 are semi-dull coal. Among them, the sample JHG-2 exhibits a uniform structure, weak asphalt luster, conchoidal fracture, and less developed fractures, while the samples JHG-4 and JHG-10 are

primary-structure coal with banded textures and irregular, stepped fracture surfaces. The samples JHG-6, JHG-7, JHG-8, and JHG-9 are semi-bright, primary-structure coals, exhibiting banded structures and stepped fracture surfaces. The macroscopic type characteristics of the $\rm L_2$ coal seam in the Juhugeng mine indicate that the lower section is mainly semi-bright coal, gradually transitioning upward to durain and semi-dull coal.

4.2 Maceral and mineral

The macerals mainly originated from plant tissues, organ residues, and degradation products (Baset et al., 1980; Hatcher and Clifford, 1997). The maceral and mineral contents are shown in Figure 2. The maceral of the $\rm L_2$ coal seam is mainly vitrinite, followed by inertinite, with the content of liptinite being the lowest. Vitrinite shows a trend of first decreasing and then increasing from bottom to top. Among them, the average vitrinite content is 68.4% (54.4%–82.7%), the average inertinite content is 27.7% (15.3%–42.2%), and the average liptinite content is 2.9% (0.8%–5.8%). The minerals mainly include clay minerals, calcite, and pyrite.

TABLE 1 Macroscopic type characteristics and R_{o,ran}.

Sample	Macroscopic type	Depth(m)	R _{o,ran} (%)
JHG-1	Durain	2.0	1.05
JHG-2	Semi-dull coal	5.0	1.09
JHG-3	Durain	8.6	0.93
JHG-4	Semi-dull coal	10.4	0.87
JHG-5	Durain	15.2	0.98
JHG-6	Semi-bright coal	18.8	0.91
JHG-7	Semi-bright coal	22.5	0.96
JHG-8	Semi-bright coal	24.1	0.96
JHG-9	Semi-bright coal	31.2	0.89
JHG-10	Semi-dull coal	34.9	1.01

4.2.1 Vitrinite

Vitrinite is the predominant maceral in bituminous coal, mainly formed by roots, stems, and woody tissues composed of lignin and cellulose (International Committee for Coal and Organic Petrology, 1998). Under oil-immersed reflected light, vitrinite usually appears dark gray or grayish black (Dai et al., 2021a). Vitrinite dominates the maceral composition (Table 2). The content of collotelinite is the highest in the $\rm L_2$ coal seam, followed by telinite and collodetrinite, while the contents of vitrodetrinite and corpogelinite are relatively low. The average collotelinite content is 21.3% (9.9%–45.1%), the average collodetrinite content is 19.0% (11.2%–26.9%), the average telinite content is 17.2% (8.1%–24.7%), the average vitrodetrinite content is 10.8% (6.5%–18.9%), and the average corpogelinite content is 0.08%.

Telinite typically displays intact cell cavities that are infilled with clay minerals or other minerals, with the cavities appearing flattened and irregular in shape (Figures 3a,b). Collotelinite exhibits a simple morphology with an indistinct internal structure (Figure 3c). Corpogelinites are often distributed in groups of circles and ellipses with clear contours (Figure 3d). Due to the particularity of its cause, the content of corpogelinite was relatively low and was only detected in a few samples. The surface of collodetrinite usually adheres to some irregular clay minerals, usually showing porphyritic structures. Compared with collotelinite, collodetrinite lacks structural continuity (Figure 3e). Vitrodetrinite usually exists in a dispersed form of discrete small particles (Figure 3f).

4.2.2 Inertinite

Inertinite is derived from plant tissues that have undergone varying degrees of oxidation and biochemical degradation during peat accumulation (Dai et al., 2021b). Inertinite usually appears white or yellowish-white under oil-immersed reflected light and has protrusions of varying degrees. It usually exhibits positive protrusions outside micrinite under the optical microscope (International Committee for Coal and Organic Petrology, 2001).

Inertinite is mainly composed of inertodetrinite and semifusinite, followed by fusinite, and the contents of micrinite, secretinite, and macrinite are relatively low. The average inertodetrinite content is 11.1% (3.0%–15.3%), the average semifusinite content is 9.1% (2.5%–14.1%), the average fusinite content is 4.8% (1.6%–15.3%), the average micrinite content is 1.73%, the average macrinite content is 0.9%, and the average secretinite content is 0.1%.

The lignofibrous tissues of plants accumulate together through fusainization during peatification to form fusinite (Jones et al., 1991; Scott, 1989; Seyler, 1928). The cell cavity of fusinite is usually empty and occasionally filled with gelinite or minerals (Dai et al., 2015). The fusinite morphology shows regular and well-preserved tissues or arc-shaped fragments (Figures 4a–c). The fusainization effect of semifusinite is weaker than that of fusinite (Smith and Cook, 1980); therefore, the cell structure of semifusinite is poorly preserved, and the cell cavity is blurred (Figure 4b).

Inertodetrinite usually exists in the form of dispersed particles and inertinite debris of different shapes (Figure 4d). The shape of secretinite is usually round or oval, with no obvious plant structure (Figure 4e). The surface protrusions of macrinite vary greatly, but the protrusions of macrinite are lower than those of secretinite in the same sample (Figure 4f). The particle size of micrinite is relatively small, and they usually exist in the form of independent fine particles or particle aggregates (Figures 4g–i).

4.2.3 Liptinite

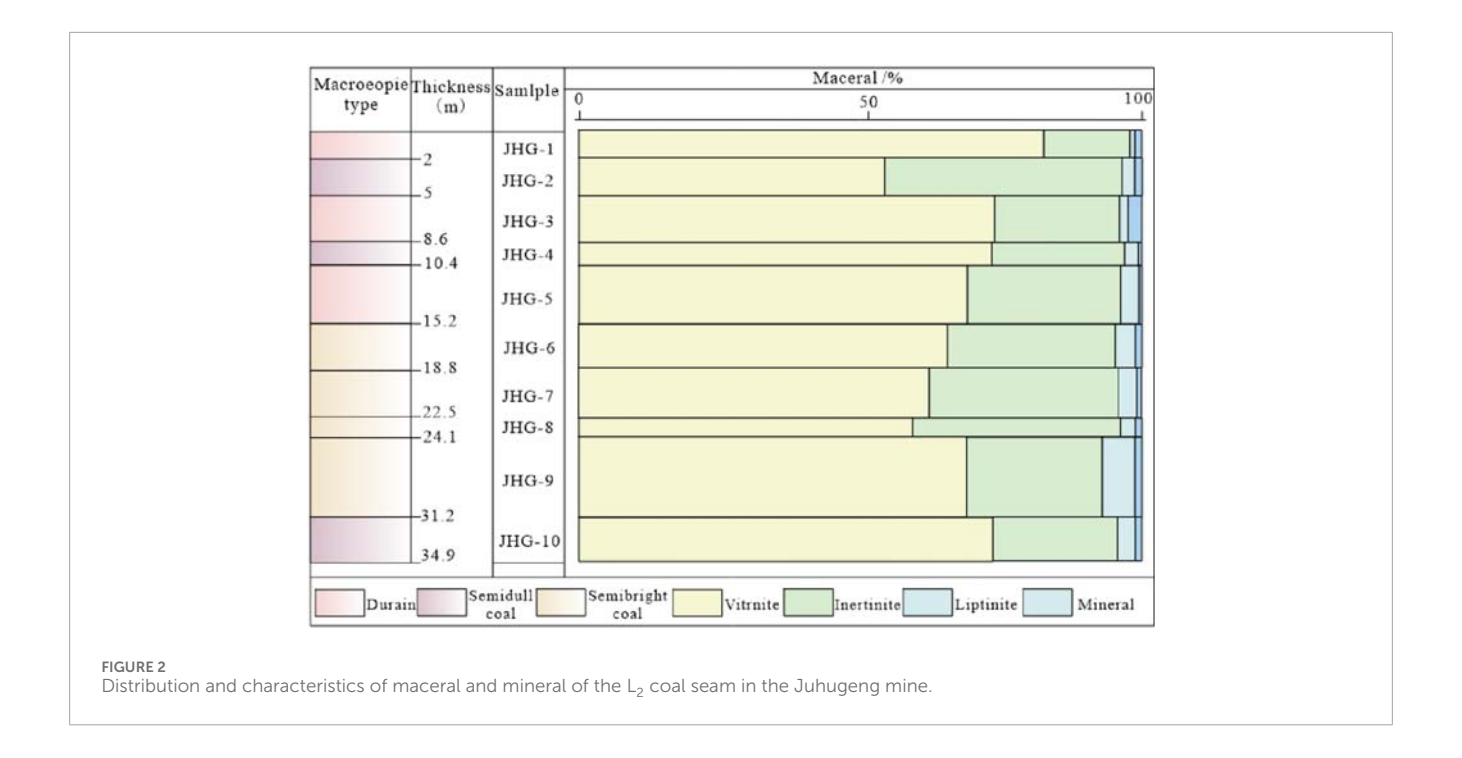
Liptinite is the maceral with the lowest reflectance, derived from non-saprophytic plant tissues (Pickel et al., 2017; Taylor et al., 1998). Liptinite appears black or dark gray under reflected light and green-yellow or orange under fluorescence (Dai et al., 2021c). The liptinite content is relatively low in the $\rm L_2$ coal seam, consisting of extremely small amounts of sporinite and cutinite. The average sporinite content is 2.8% (0.8%–5.5%), while cutinite is detected in only one sample.

Sporinite is mainly formed from plant spores and pollen exine (Pickel et al., 2017) and is mostly flat ring-shaped, flat closed ring-shaped, or worm-like (Figures 5a,b). Cutinite mainly originates from the outer protective layers of plant leaves, young branches, and thin stems (Dai et al., 2021c). Cutinite is present as long strips in the cross-section of the vertical layering (Figure 5c).

4.2.4 Mineral

The formation of coal has undergone a complex geological process. Due to its complex and diverse composition, the types and occurrence characteristics of minerals in coal can provide valuable insights into the coal-forming environment, sediment environment, and sediment source (Ward, 2016; Finkelman et al., 2019). The minerals mainly include clay minerals, calcite, and pyrite (Table 2), with pyrite content ranging from 0.2% to 1.7%, clay mineral content from 0.2% to 1.0%, and calcite content from 0.5% to 0.8%.

The clay minerals appear grayish black or black under oil-immersed reflected light, with diverse distribution patterns, filling the cell cavities of telinite or dispersed on the surface of collodetrinite (Figure 3e). Calcite is usually filled in fissures (Figures 6a–c). Pyrite is a common sulfide mineral in coal. In this study, pyrite is mostly fine-grained dispersed pyrite (Figures 6d,e) and disseminated pyrite (Figure 6f). The dispersed granular pyrite



exhibits relatively smooth, uniform surfaces and variable grain sizes and is predominantly distributed in collodetrinite.

5 Discussion

5.1 Maceral indices

The sedimentary environment of peat bogs during coal formation can be restored through maceral indices (Sen, 2016). The peat swamp environment is mainly composed of water bodies and peat, and the dynamic relationship between these components governs the composition and structure of the resulting coal, ultimately affecting its chemical and physical properties (Moore, 1989). The processes of gelification and fusainization are affected by coal-forming plants, the degree of water coverage, and hydrodynamic conditions, thereby influencing the changes in maceral and mineral contents (Crosdale, 1993; Dehmer, 1995; Moore and Shearer, 2003; Diessel, 2007; Lu et al., 2017; Dai et al., 2020).

The commonly used coal facies indices include GI, TPI, VI, GWI, V/I, and T–D–F relationship diagrams (Harvey and Dillon, 1985; Diessel, 1986; Calder et al., 1991; Silva and Kalkreuth, 2005; Guatame and Rincón, 2021). In this study, the GI–TPI, GWI–VI, and T–D–F relationship diagrams were used to analyze coal facies characteristics (Table 3).

5.1.1 GI-TPI relationship diagram

The GI-TPI diagram, as proposed by Diessel (1982), Diessel (1986), and Diessel (2007), is a widely used tool for reconstructing peat swamp environments during coal formation. The TPI indicates the degree of degradation of plant tissues and the proportion of woody plants in the original coal-forming plants. Therefore, a TPI value of 1 represents the boundary between forest and low

swamps. Similarly, a GI value of 1 marks the transition between wet and dry swamp, serving as a key indicator for distinguishing peat swamp types. According to the GI-TPI relationship diagram, the coal-forming environment was classified into three major types of coal facies—low swamp, wet forest swamp, and dry forest swamp (Diessel, 1986). The parameters are calculated using Equations 1, 2.

$$GI = (TotalV + Ma)/(SF + F + ID), \tag{1}$$

$$TPI = (T + CT + F + SF)/(CD + Ma + VD).$$
 (2)

It can be known from Figure 7 that the average GI value is 3.17 (1.35–5.92). The samples are distributed in the wet forest swamp, indicating that the peat swamp environment is relatively stable overall (Diessel, 1986). The GI value is $1 < {\rm GI} < 10$ in the ${\rm L}_2$ coal seam, indicating that the water coverage degree of the swamp environment is relatively deep. TPI > 1 indicates that the plant structure of the coal seam is well preserved and the degradation degree is low, reflecting that the coal-forming plants are a mixture of grass and trees. The ${\rm L}_2$ coal seam is mainly composed of woody plants, except for the JHG-9 sample, which contains mainly herbaceous plants. Such maceral-based facies characterization is critical not only for paleoenvironmental reconstruction but also for evaluating the petrophysical behavior of organic-rich strata (Fathy et al., 2025).

5.1.2 GWI-VI relationship diagram

The GWI-VI relationship diagram is established through GWI and VI, where VI = 1 serves as the boundary between herbaceous plants and woody plants and GWI = 1 distinguishes the boundary between forest and flowing swamps (Calder et al., 1991). A lower GWI value reflects weaker hydrodynamic conditions. The calculations are shown in Equations 3, 4.

$$GWI = (CG + TotalM + VD)/(T + CT + CD),$$
(3)

TABLE 2 Maceral and mineral contents in the Juhugeng mine (%).

Maceral	JHG-1	JHG-2	JHG-3	JHG-4	JHG-5	JHG-6	JHG-7	JHG-8	JHG-9	JHG-10
Т	18.3	11.7	8.1	16.4	24.5	14.7	16.4	24.7	15.2	21.7
СТ	45.1	15.3	30.9	22.2	9.9	18.8	19.9	12.0	11.3	27.9
CD	11.2	17.1	16.1	22.4	23.4	22.2	19.1	16.1	26.9	14.9
CG	_	0.4	_	_	_	_	0.2	_	_	0.2
VD	8.2	9.9	18.9	12.4	11.5	9.7	6.8	6.5	15.6	8.7
Total-V	82.7	54.4	73.9	73.4	69.3	65.4	62.3	59.4	69.0	73.5
F	1.6	15.3	2.1	1.9	4.6	6.0	3.5	5.7	4.4	2.6
SF	2.5	9.9	6.7	7.1	9.9	10.9	13.5	14.1	11.5	5.3
Sec	_	_	0.0	0.2	_	0.6	_	0.2	_	_
Ma	_	0.2	0.2	1.4	0.5	0.4	0.4	1.2	4.4	0.4
Mi	1.3	1.4	3.4	3.6	3.5	1.2	1.4	0.4	0.9	_
ID	9.9	15.3	9.9	9.5	8.6	10.9	14.8	15.3	3.0	13.9
Total-I	15.3	42.2	22.3	23.6	27.1	30.0	33.6	36.9	24.1	22.2
Sp	0.8	2.3	1.4	2.4	3.2	3.4	3.3	2.7	5.5	3.2
Cut	_	_	_	_	_	0.2	_	_	0.2	_
Total-L	0.8	2.3	1.4	2.4	3.2	3.6	3.3	2.7	5.7	3.2
Ру	_	0.4	1.7	0.2	0.2	_	_	_	0.2	0.2
Cm	0.4	0.7	0.2	0.3	0.3	1.0	0.8	1.0	0.9	0.9
Ca	0.8	_	0.5	_	_	_	_	_	_	_
Total-M	1.2	1.1	2.4	0.5	0.5	1.0	0.8	1.0	1.1	1.1

T, telinite; CT, collodelinite; CD, collodelrinite; CG, corpogelinite; VD, vitrodetrinite; Total-V, total vitrinites; F, fusinite; SF, semifusinite; Sec, secretinite; Ma, macrinite; ID, inertodetrinite; Total-I, total inertinites; Sp, sporinite; Total-L, total liptinites; Py, pyrite; Cm, clay minerals; Ca, calcite; Total-M, total minerals.

$$VI = (T + CT + CG + SF + F)/(CD + Sp + Cut + ID + VD).$$
 (4)

The average GWI value is 0.21 (0.13–0.39), suggesting relatively weak groundwater dynamics during peat accumulation (Calder et al., 1991) (Figure 8). The corresponding bog water has a relatively low nutrient level and is ombrotrophic. The VI value is generally greater than 1, indicating that the coal-forming plants are mainly woody.

5.1.3 T-D-F relationship diagram

Silva and Kalkreuth (2005) established the T-D-F relationship diagram by statistically analyzing the values of T*, D*, and F*parameters to classify coal facies types. According to the T-D-F relationship diagram, the samples are classified into three major types of coal facies. High T*values reflect wet forest swamps, high D*values reflect open swamps, and high F*values reflect terrestrial

forest swamps (Marchioni and Kalkreuth, 1991). The calculations are shown in Equations 5–7.

$$T^* = T + CT, (5)$$

$$D^* = VD + Sp + Cut + ID + Cm, (6)$$

$$F^* = SF + F. (7)$$

The L_2 coal seam is mainly located in the wet forest marsh area. The T*values ranged from 33.78% to 73.33%, with an average of 49.28% (Figure 9), indicating that the peat swamp environment was mainly characterized by a humid climate (Silva and Kalkreuth, 2005). The F*values ranged from 4.76% to 31.53%, with an average of 18.15%. It reflects that the peat swamp environment is, to some extent, affected by the dry climate, with D*values ranging from

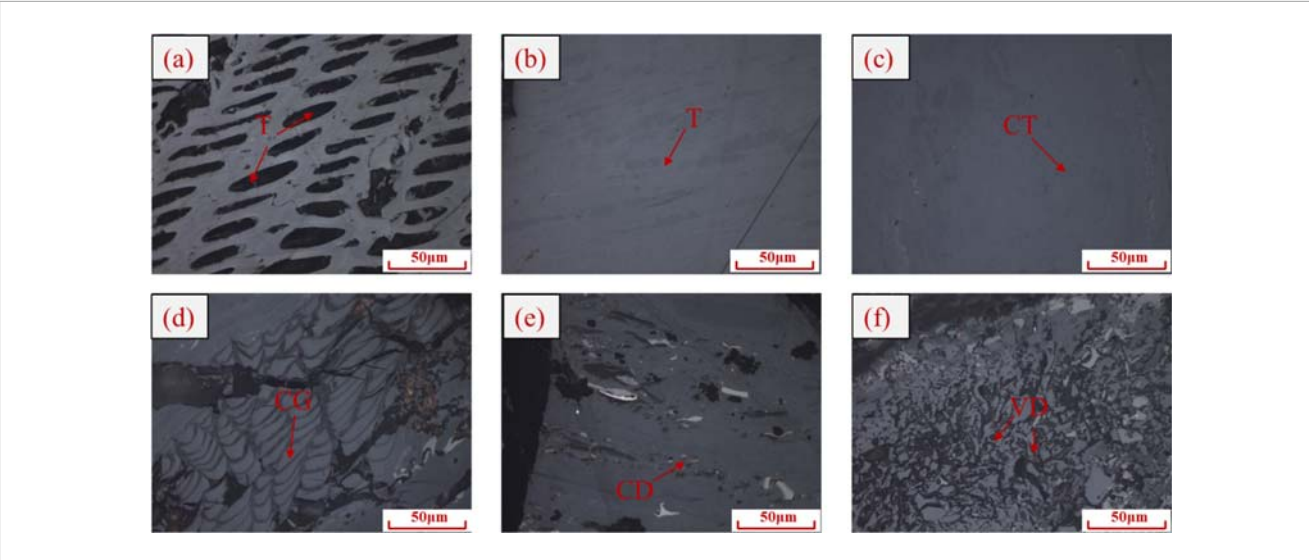
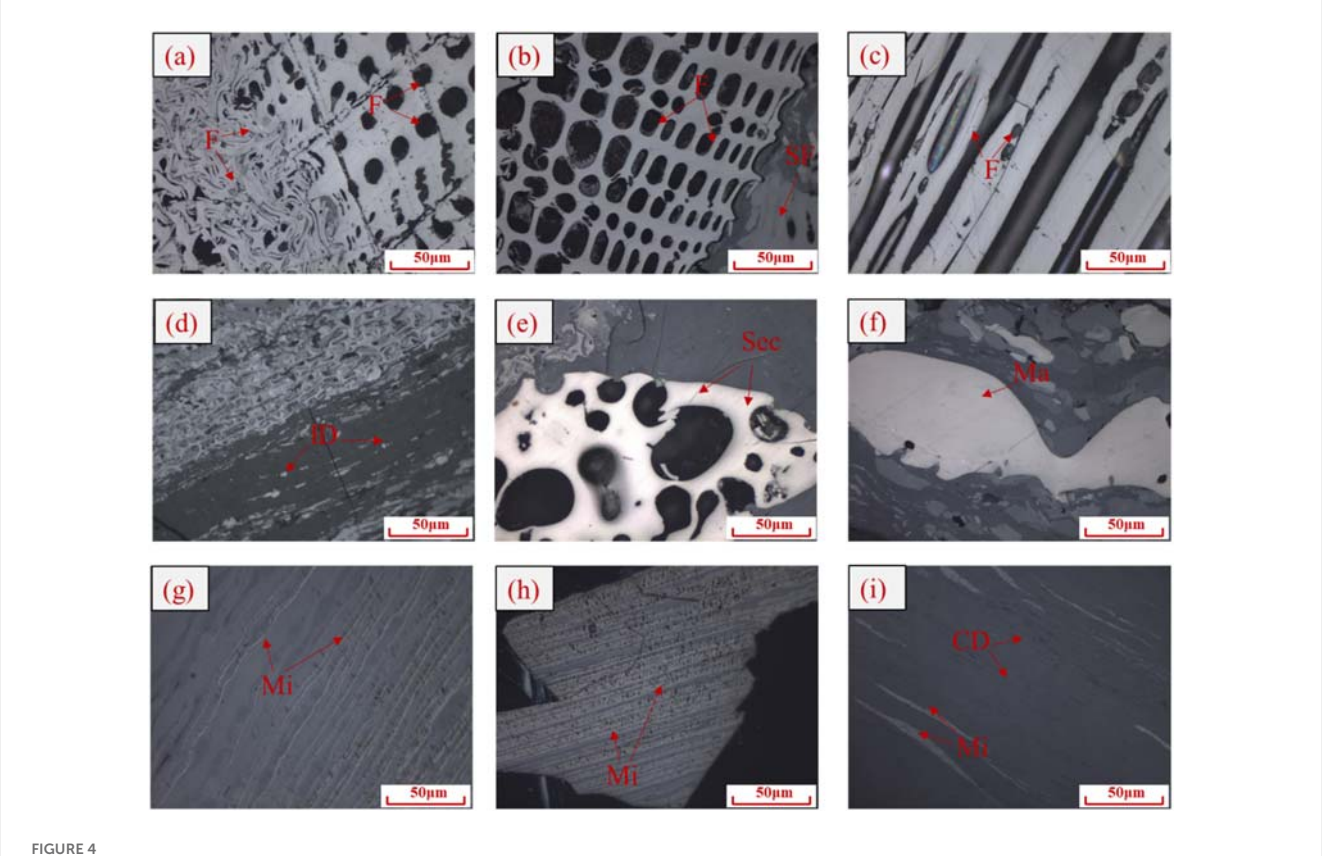


FIGURE 3
Characteristics of vitrinite under an optical microscope in oil-immersed reflected light (a), (b) telinite, (c) collotelinite, (d) corpogelinite, (e) collodetrinite, and (f) vitrodetrinite.



Characteristics of inertinite under an optical microscope in oil-immersed reflected light: (a) fusinite, (b) fusinite and semifusinite, (c) fusinite, (d) Inertodetrinite, (e) secretinite, (f) macrinite, and (g-i), micrinite.

21.9% to 38.9% (32.58% on average), indicating that the coal-accumulation area has received a relatively smaller supply of external debris materials (Marchioni and Kalkreuth, 1991).

5.1.4 V/I and GI values

The extent of water coverage in coal-forming bogs has a strong influence on the oxidation–reduction properties of peat bogs.

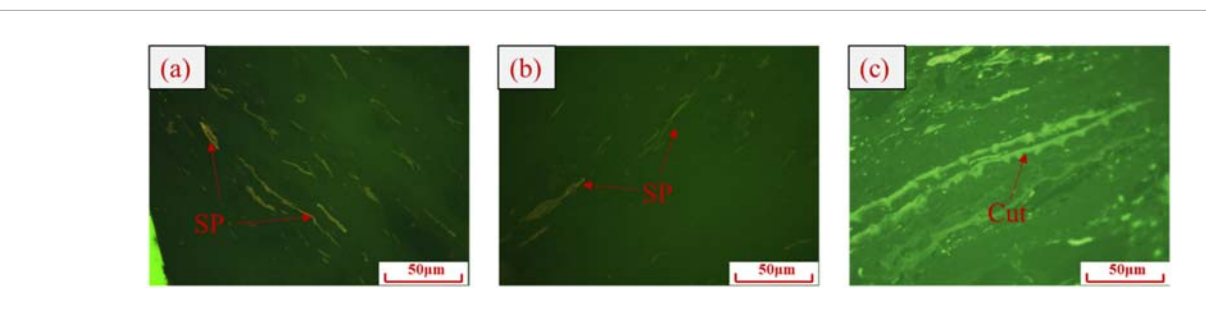


FIGURE 5
Characteristics of liptinite under an optical microscope in fluorescence (a,b) sporinite, and (c) cutinite.

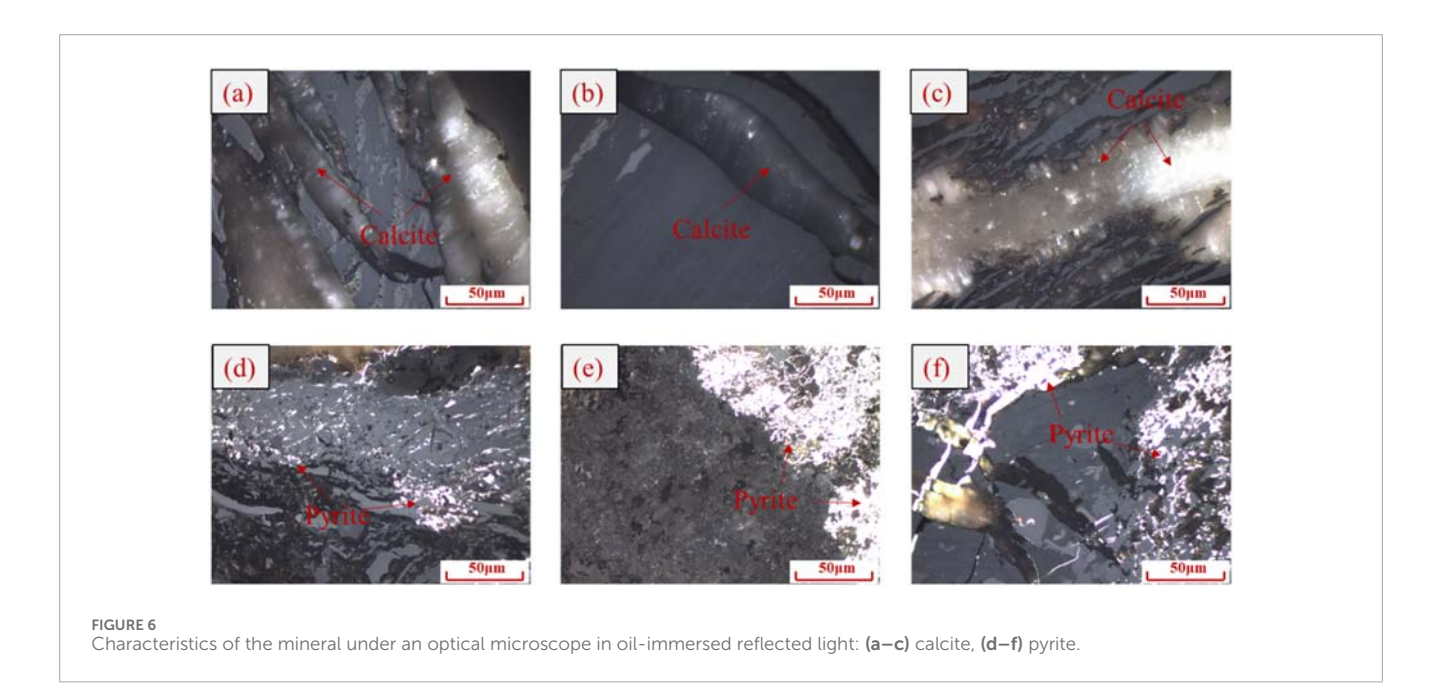
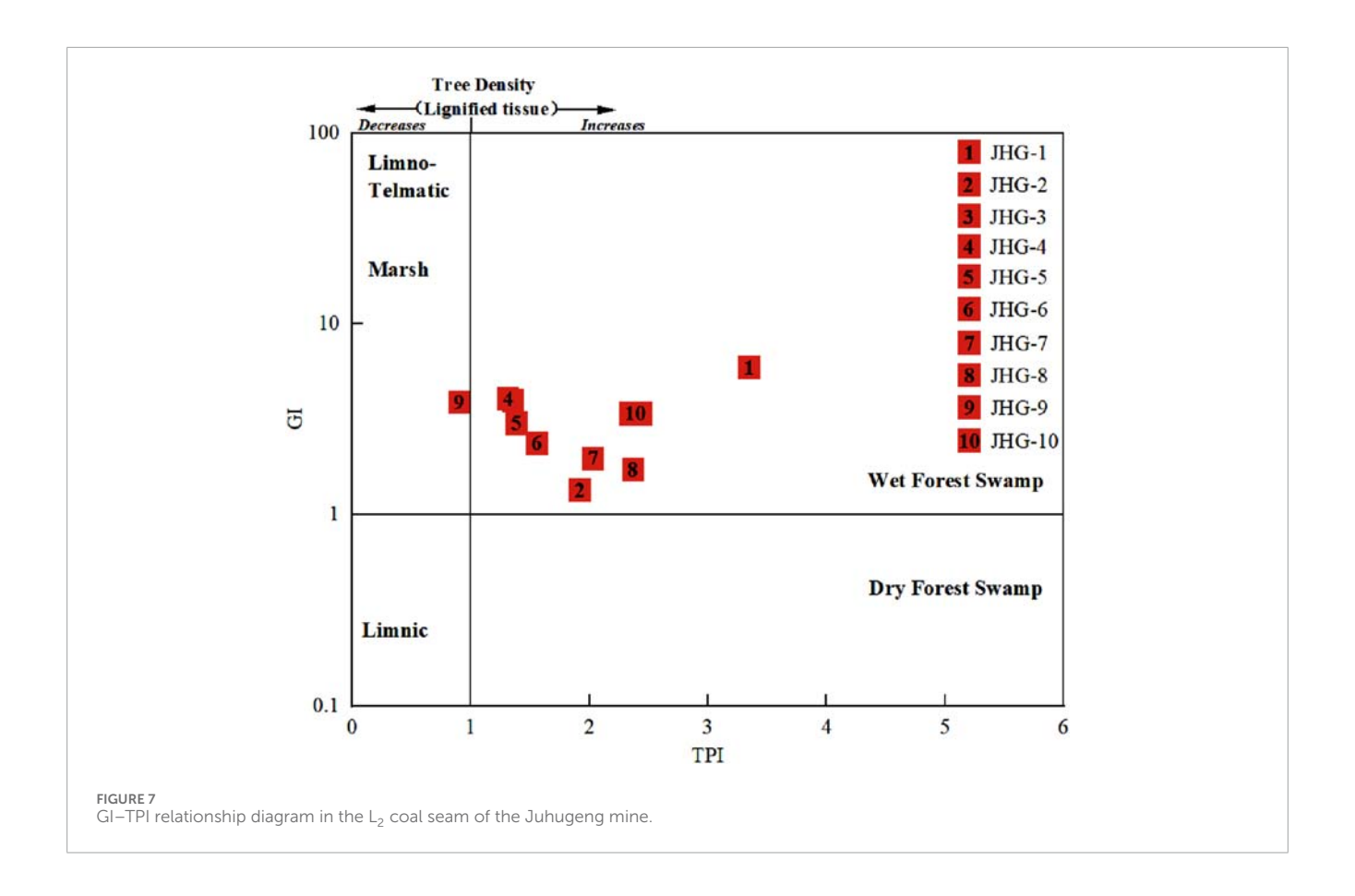


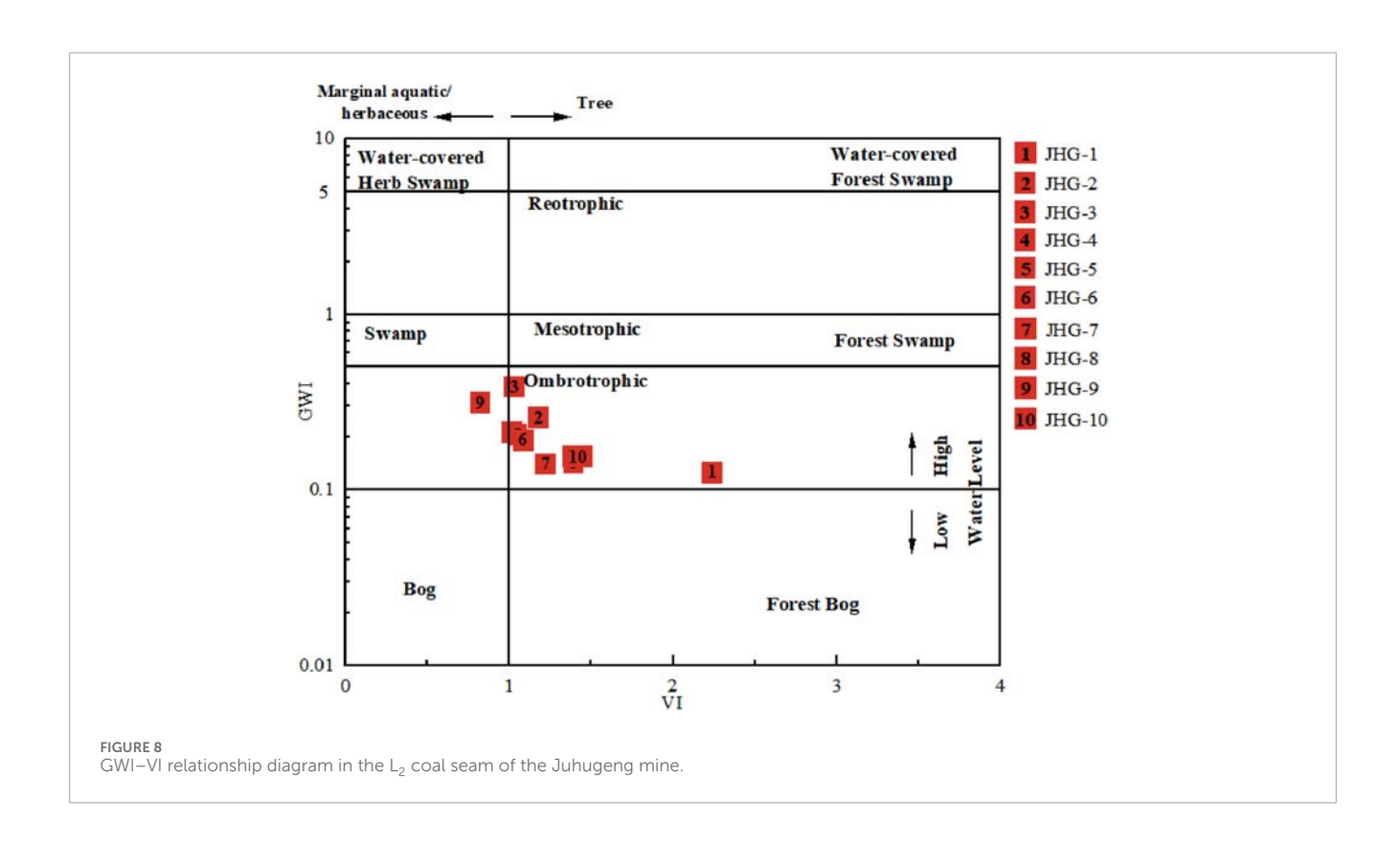
TABLE 3 Coal facies indices of L_2 coal in the Juhugeng mine.

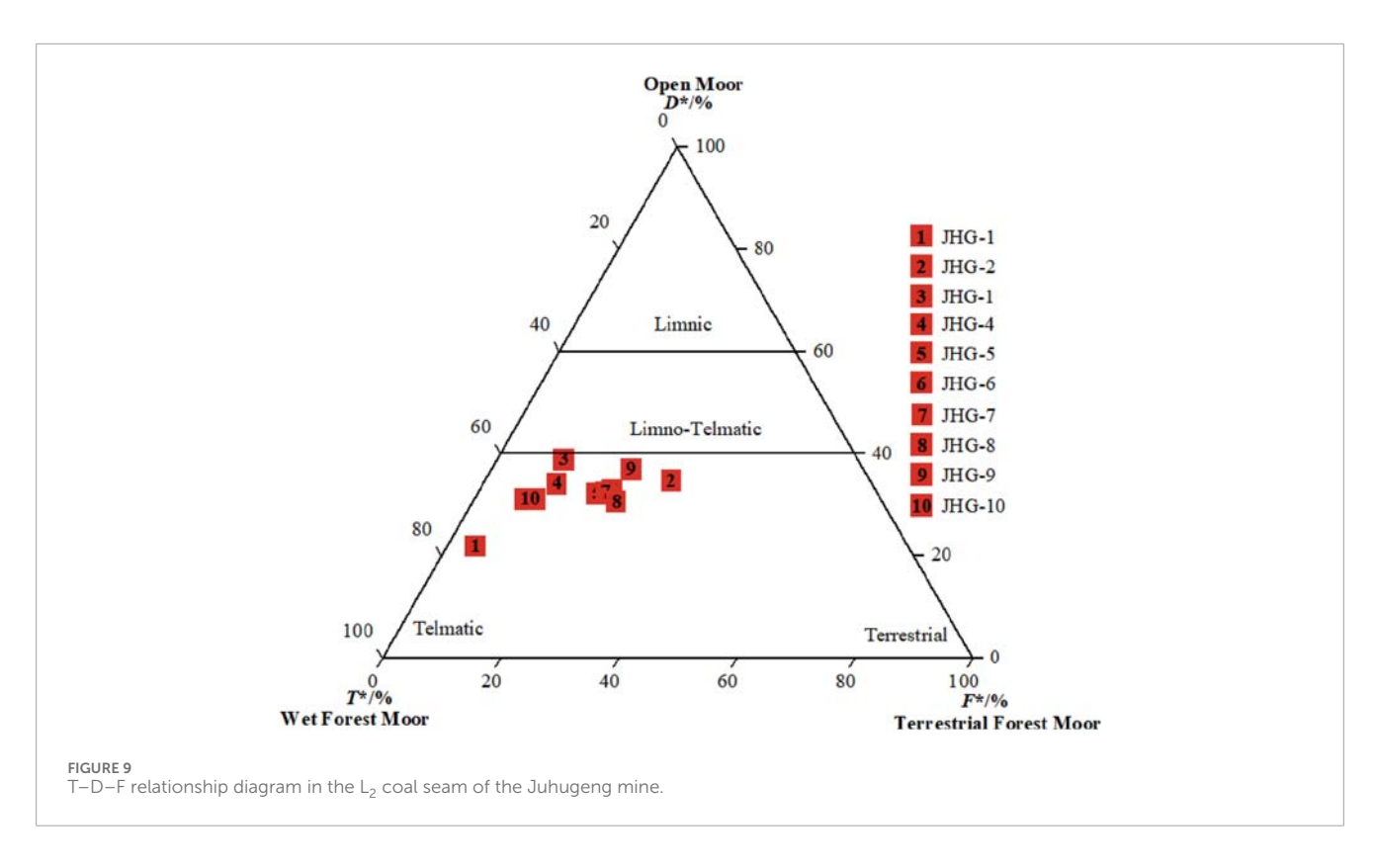
Sample	Gl	TPI	VI	GWI	V/I
JHG-1	5.92	3.35	2.24	0.13	5.41
JHG-2	1.35	1.92	1.18	0.26	1.29
JHG-3	3.96	1.36	1.03	0.39	3.32
JHG-4	4.06	1.31	1.02	0.21	3.11
JHG-5	3.02	1.39	1.05	0.21	2.56
JHG-6	2.37	1.56	1.09	0.19	2.19
JHG-7	1.97	2.03	1.22	0.14	1.85
JHG-8	1.73	2.37	1.39	0.14	1.61
JHG-9	3.89	0.90	0.83	0.31	2.86
JHG-10	3.40	2.39	1.42	0.16	3.32

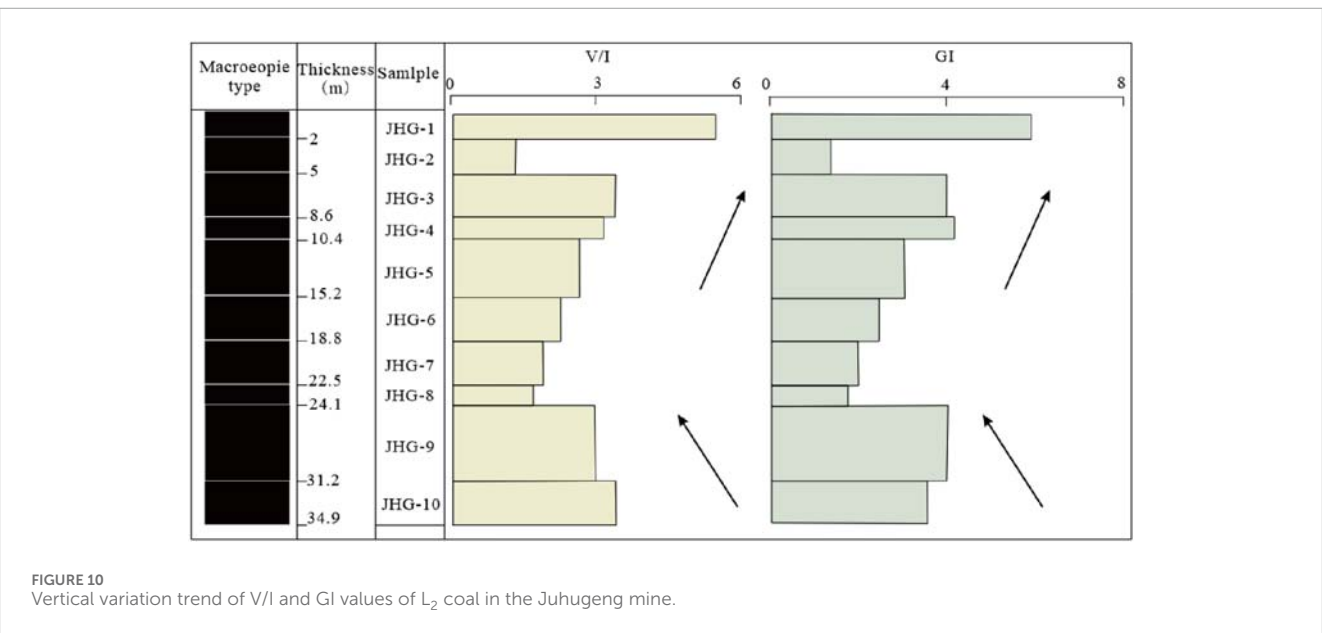
Accordingly, the V/I value is commonly applied to visually reflect the oxidation–reduction conditions of the bog. Generally, a moist reducing environment is conducive to the formation of vitrinite, and a dry oxidizing environment is conducive to the formation of inertinite (Harvey and Dillon, 1985).

The average V/I value is 2.75 (1.29–5.41), reflecting that the peat swamp environment was mainly highly humid, water-covered, and reducing. The cyclicity of thick coal seams is classified using indicators that reflect the degree of water coverage in ancient peat bogs through V/I and GI values. The GI value reflects the water level changes in ancient peat bogs and the degree of gelation of plants. A high GI value represents a relatively high level of water coverage, while a low GI value indicates the opposite. From the base of the coal seam up to 22.5 m, the V/I and GI indices decrease, indicating a reduced degree of rehydration. The growth rate of peat is less than that of the submerged surface, and the gelation intensity decreases, reflecting a process of water regression. Similarly, above 22.5 m, the processes of water advancement are observed (Figure 10).







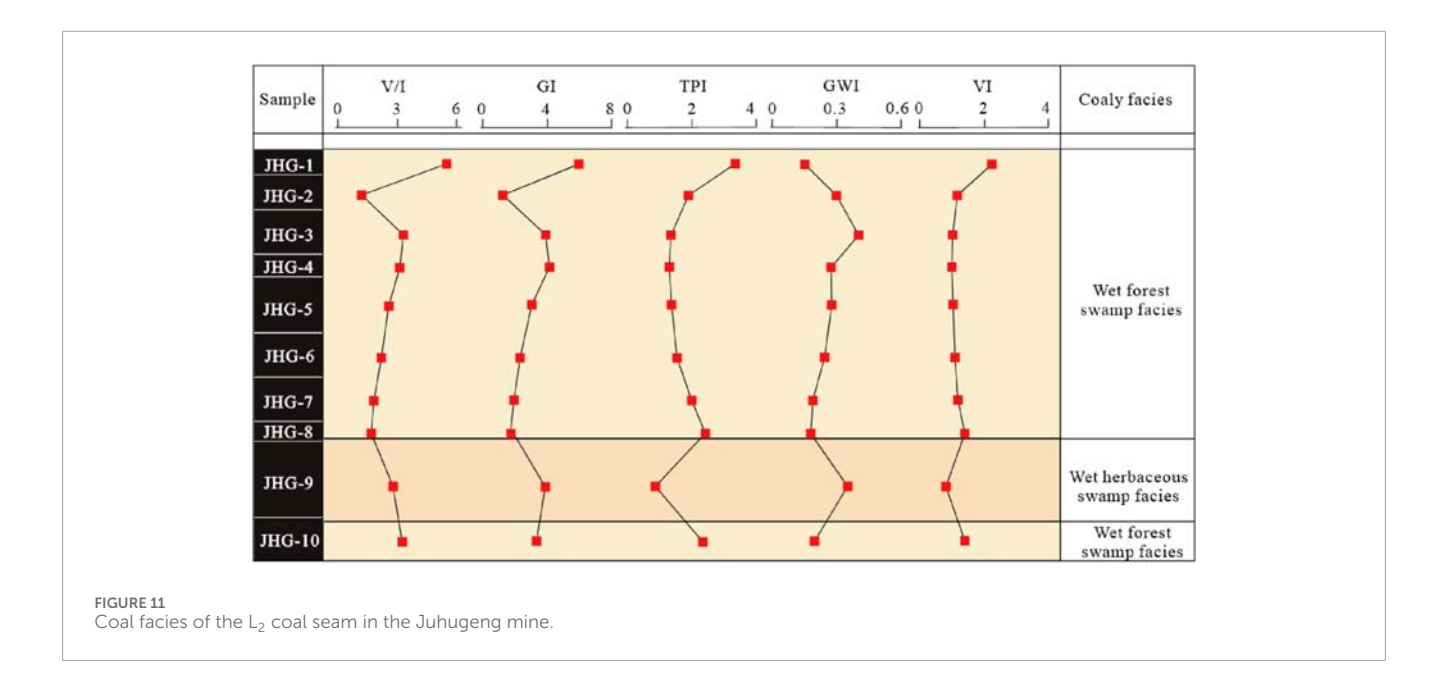


5.2 Vertical evolution characteristics of coal facies

The coal facies include the wet forest swamp and the wet herbaceous swamp in the Juhugeng mine. The L_2 coal seam has undergone an evolution from bottom to top from the wet forest swamp to the wet herbaceous swamp and then to the wet forest swamp (Figure 11). This cyclic facies evolution likely reflects

shifts in regional hydrological conditions and climate-induced vegetation changes (Jamaluddin et al., 2024).

Stage I: JHG-10 is a wet forest swamp facies. VI > 1 and TPI>1 indicate that the coal-forming plants are mainly woody. The macroscopic type is semi-dull coal, with a GI value of 3.40 and a V/I value of 3.32, reflecting the depth of the marsh cover and indicating a strongly water-covered environment. The GWI value of 0.16 reflects weak



groundwater dynamics, limited recharge, and an overall low trophic level.

Stage II: The JHG-9 sample is a wet herbaceous swamp facies. VI < 1 and TPI<1 indicate that coal-forming plants are mainly herbaceous. The macroscopic type is semibright coal, with a GI value of 3.89 and a V/I value of 2.86. The overlying water is slightly shallower, still in a strongly overlying water environment, with a high degree of gelation and a slightly increased groundwater recharge.

Stage III: The JHG-8 to JHG-1 samples are in the wet forest swamp facies. VI > 1 and TPI>1 indicate that the coal-forming plants are mainly woody. The macroscopic types have transitioned from semi-bright coal to semi-dull coal and durain. The average GI value is 3.05 (1.35–5.92). The V/I average value is 2.67 (1.29–5.41). Compared with the previous swamp, the water coverage changes little, ranging from strong water cover to weak water cover. The average GWI is 0.21 (0.13–0.39), suggesting generally stagnant groundwater conditions, although both groundwater dynamics and marsh water fluidity increased toward the end of peat accumulation.

The Muli basin is located within the Qilian fault uplift zone of the Qilian orogenic belt (Shang et al., 2018), and its tectonic background has a profound influence on the development of coal seams and facies evolution. The Qilian tectonic movements, particularly during the Caledonian and Mesozoic periods, shaped a compound syncline structure in the Juhugeng mine and led to differential subsidence across the basin. The alternating uplifts and depressions, along with thrust–fault-induced flexural subsidence, periodically increased accommodation space for peat accumulation (Wen et al., 2011; Pan et al., 2009). This dynamic tectonic backdrop explains the vertical facies shift observed in the L₂ coal seam: episodes of enhanced subsidence likely favored thick, waterlogged forest swamps (stages I and III), while tectonic uplift or reduced subsidence may have temporarily lowered the

water table, resulting in the development of herbaceous swamps (Stage II). Furthermore, the steep-inversion folding and synclinal compression in the southern part of the mine may have contributed to local variations in hydrological stability and sediment supply, which are reflected in the facies index fluctuations (GWI and VI). These structural influences underscore the strong coupling between tectonic evolution, basin hydrodynamics, and peat-forming environments in the Muli coalfield.

The analysis of coal petrology and facies evolution not only provides insights into the paleoenvironmental reconstruction but also serves as a critical foundation for evaluating coalbed methane potential, optimizing mining strategies, and promoting the clean and efficient utilization of coal resources. Therefore, understanding the maceral composition and depositional conditions of the $\rm L_2$ coal seam holds significant implications for both geological research and practical resource development in the Muli coalfield.

6 Conclusion

- 1. The macroscopic type of the $\rm L_2$ coal seam in the Juhugeng mine is mainly semi-bright coal at the bottom of the coal seam, gradually transitioning to durain and semi-dull coal toward the top. The $\rm L_2$ coal seam is mainly vitrinite, followed by inertinite. The liptinite and mineral contents are relatively low.
- 2. The GI-TPI and GWI-VI relationship diagrams indicate that the plant structure is well preserved, and the coalforming plants are mainly woody. The T-D-F relationship diagram reflects that the peat swamp environment is mainly characterized by a humid climate and is affected, to a certain extent, by a dry climate. The V/I value indicates that the peat swamp environment is mainly in a highly humid, watercovered, reducing environment.
- 3. By comprehensively analyzing multiple coal facies indicators, the sedimentary period of the L₂ coal seam is shown to undergo evolution stages from wet forest swamp facies to wet

herbaceous swamp facies and back to wet forest swamp facies. The L_2 coal seam changes from the bottom wet forest swamp facies to the middle and lower wet herbaceous swamps and finally to the wet forest swamp facies.

4. The vertical alternation of coal facies in the L_2 coal seam reflects paleoclimate-induced vegetation shifts, with cyclic transitions between woody and herbaceous assemblages indicating periodic fluctuations under hydrological conditions and mire ecosystems. Such rhythmic alternations in peatforming vegetation and the hydrological regime likely record Milankovitch-scale climate oscillations or regional tectonosedimentary influences that shaped the peat accumulation environment.

Data availability statement

The original contributions presented in the study are included in the article/supplementary material; further inquiries can be directed to the corresponding author.

Author contributions

JL: Methodology, Conceptualization, Writing – review and editing, Writing – original draft. LW: Writing – review and editing, Methodology.

Funding

The author(s) declare that financial support was received for the research and/or publication of this article. This work was supported

by the Fundamental Research Program of Shanxi Province (nos. 202203021221230, 202203021212475).

Conflict of interest

The authors declare that the research was conducted in the absence of any commercial or financial relationships that could be construed as a potential conflict of interest.

Generative AI statement

The author(s) declare that no Generative AI was used in the creation of this manuscript.

Any alternative text (alt text) provided alongside figures in this article has been generated by Frontiers with the support of artificial intelligence and reasonable efforts have been made to ensure accuracy, including review by the authors wherever possible. If you identify any issues, please contact us.

Publisher's note

All claims expressed in this article are solely those of the authors and do not necessarily represent those of their affiliated organizations, or those of the publisher, the editors and the reviewers. Any product that may be evaluated in this article, or claim that may be made by its manufacturer, is not guaranteed or endorsed by the publisher.

References

ASTM Standard D2798-11A (2011). Standard test method for microscopical determination of the vitrinite reflectance of coal. West Conshohocken, PA, USA: ASTM International.

Baset, Z. H., Pancirov, R. J., and Ashe, T. R. (1980). Organic compounds in coal: structure and origins. *Phys. Chem. Earth* 12, 619–630. doi:10.1016/0079-1946(79)90143-5

Calder, J. H., Gibling, M. R., and Mukhopadhyay, P. K. (1991). Peat formation in a westphalian B Piedmont setting, cumberland basin, Nova Scotia: implications for the maceral-based interpretation of rheotrophic and raised paleomires. *Contrib. Ser. No.* 91-002.

Cao, D. Y., Liu, T. J., Wang, D., Wang, T., Wen, H. J., and Pan, Y. L. (2009). Analysis of formation conditions of natural gas hydrate in muli coalfield, Qinghai province. *Coal Geol. China* 21 (9), 3–6.

Chinese National Standard GB/T 18023-2000, Standardization Administration of China (2008). Classification of macrolithotype for bituminouscoal. Beijing, China: Standard Press of China.

Chinese National Standard GB/T 482-2008, Standardization Administration of China (2008). Sampling of coal seams. Beijing, China: Standard Press of China.

Crosdale, P. J. (1993). Coal maceral ratios as indicators of environment of deposition: do they work for ombrogenous mires? An example from the Miocene of New Zealand. Org. Geochem. 20 (6), 797–809. doi:10.1016/0146-6380(93)90064-i

Dai, S., Ren, D., Li, S., Zhao, L., and Zhang, Y. (2007). Coal facies evolution of the main minable coal-bed in the Heidaigou Mine, Jungar Coalfield, Inner Mongolia, northern China. Sci. China Ser. D Earth Sci. 50 (Suppl. 2), 144–152. doi:10.1007/s11430-007-6024-z

Dai, S., Hower, J., Ward, C., Guo, W., Song, H., O'Keefe, J., et al. (2015). Elements and phosphorus minerals in the middle Jurassic inertinite-rich coals of the Muli Coalfield on the Tibetan Plateau. *Int. J. Coal Geol.* 144, 23–47. doi:10.1016/j.coal.2015.04.002

Dai, S., Hower, J., Finkelman, R., Graham, I., French, D., Ward, C., et al. (2020). Organic associations of non-mineral elements in coal: a review. *Int. J. Coal Geol.* 218, 103347. doi:10.1016/j.coal.2019.103347

Dai, S., Tang, Y., Jiang, Y., Liu, J., Ren, D., Zhao, F., et al. (2021a). An indepth interpretation of definition and classification of macerals in coal (ICCP system 1994) for Chinese researchers, I: vitrinite. *J. China Coal Soc.* 46, 1821–1832. doi:10.13225/j.cnki.jccs.2021.0419

Dai, S., Wang, S., Tang, Y., Jiang, Y., Ren, D., Zhao, L., et al. (2021b). An indepth interpretation of definition and classification of macerals in coal (ICCP system 1994) for Chinese Researchers, II: inertinite. *J. China Coal Soc.* 46, 2212–2226. doi:10.13225/j.cnki.jccs.2021.0420

Dai, S., Zhao, L., Tang, Y., Ren, D., Wei, Q., Jiang, Y., et al. (2021c). An indepth interpretation of definition and classification of macerals in coal (ICCP system 1994) for Chinese researchers, IV: liptinite. *J. China Coal Soc.* 46 (9), 2965–2983. doi:10.13225/j.cnki.jccs.2021.0422

Dehmer, J. (1995). Petrological and organic geochemical investigation of recent peats with known environments of deposition. *Int. J. Coal Geol.* 28 (2-4), 111-138. doi:10.1016/0166-5162(95)00016-x

Diessel, C. F. K. (1982). An appraisal of coal facies based on maceral characteristics. Aust. Coal Geol. 4 (2), 474–484.

Diessel, C. F. K. (1986). "On the correlation between coal facies and depositional environments," in *Proceeding 20th symposium of department geology* (New South Wales: University of New Castle), 19–22.

Diessel, C. F. (2007). Utility of coal petrology for sequence-stratigraphic analysis. *Int. J. Coal Geol.* 70 (1-3), 3–34. doi:10.1016/j.coal.2006.01.008

Diessel, C. F., and Diessel, C. F. (1992). "Coal facies and depositional environment," in Coal-bearing depositional systems, 161–264.

- Fathy, D., Lee, E. Y., Xiang, X., Fathi, E., and Sami, M. (2025). Petrophysical properties of the middle Miocene sediments on the central gulf of Suez, Egypt. *Front. Earth Sci.* 13, 1592041. doi:10.3389/feart.2025.1592041
- Feng, S., He, J., Tian, J., Lu, X., and Yang, B. (2019). The characteristic and evolution of coal-forming swamp in hanshuiquan district, santanghu coalfield, Xinjiang, NW China, during the Middle Jurassic: evidence from coal petrography, coal facies and sporopollen. *Int. J. Coal Sci. & Technol.* 6 (1), 1–14. doi:10.1007/s40789-018-0230-5
- Finkelman, R. B., Dai, S., and French, D. (2019). The importance of minerals in coal as the hosts of chemical elements: a review. *Int. J. Coal Geol.* 212, 103251. doi:10.1016/j.coal.2019.103251
- Gmur, D., and Kwiecińska, B. K. (2002). Facies analysis of coal seams from the cracow sandstone series of the upper silesia Coal basin, Poland. *Int. J. Coal Geol.* 52 (1-4), 29–44. doi:10.1016/s0166-5162(02)00101-5
- Guatame, C., and Rincón, M. (2021). Coal petrology analysis and implications in depositional environments from upper Cretaceous to Miocene: a study case in the Eastern Cordillera of Colombia. *Int. J. Coal Sci. & Technol.* 8 (5), 869–896. doi:10.1007/s40789-020-00396-z
- Harvey, R. D., and Dillon, J. W. (1985). Maceral distributions in Illinois coals and their paleoenvironmental implications. *Int. J. Coal Geol.* 5 (1-2), 141–165. doi:10.1016/0166-5162(85)90012-6
- Hatcher, P.~G., and~Clifford, D.~J.~(1997).~The~organic~geochemistry~of~coal:~from~plant~materials~to~coal.~Org.~Geochem.~27~(5-6), 251-274.~doi:10.1016/s0146-6380(97)00051-x
- Huo, T., Liu, S., Qi, W., Zhu, K., Wang, J., and Tan, F. (2020). Geochemistry characteristics and indicative significance of rare earth elements in coal from juhugeng coal district, the muli coalfield in Qinghai province. *Geol. Bull. China* 39 (7), 995–1005.
- International Committee for Coal and Organic Petrology (ICCP) (1998). The new vitrinite classification (ICCP system 1994). Fuel 77 (5), 349–358. doi:10.1016/S0016-2361(98)80024-0
- International Committee for Coal and Organic Petrology (ICCP) (2001). The new inertinite classification (ICCP system 1994). *Fuel* 80 (4), 459–471. doi:10.1016/S0016-2361(00)00102-2
- Jamaluddin, J., Schöpfer, K., Wagreich, M., Gier, S., and Fathy, D. (2024). Effect of depositional environment and climate on organic matter enrichment in sediments of the upper Miocene-Pliocene kampungbaru formation, lower kutai basin, Indonesia. *Geosciences* 14 (6), 164. doi:10.3390/geosciences14060164
- Jiu, B., Huang, W., and Hao, R. (2021). A method for judging depositional environment of coal reservoir based on coal facies parameters and rare Earth element parameters. *J. Petroleum Sci. Eng.* 207, 109128. doi:10.1016/j.petrol.2021.109128
- Jones, T., Scott, A., and Cope, M. (1991). Reflectance measurements and the temperature of formation of modern charcoals and implications for studies of fusain. *Bull. la Société Géologique Fr.* 162 (2), 193–200.
- Kalkreuth, W. D. (2004). Coal facies studies in Canada. *Int. J. Coal Geol.* 58 (1-2), 23–30. doi:10.1016/j.coal.2003.06.001
- Kumar, A., Singh, A. K., Paul, D., and Kumar, A. (2020). Evaluation of hydrocarbon potential with insight into climate and environment present during deposition of the sonari lignite, barmer basin Rajasthan. *Energy Clim. Change* 1, 100006. doi:10.1016/j.egycc.2020.100006
- Kumar, A., Singh, A. K., Paul, D., and Kumar, A. (2021). Paleoenvironmental, paleovegetational, and paleoclimatic changes during Paleogene lignite formation in Rajasthan, India. *Arabian J. Geosciences* 14 (22), 2350. doi:10.1007/s12517-021-08638-3
- Kumar, A., Singh, A. K., and Christanis, K. (2024). Paleodepositional environment and hydrocarbon generation potential of the Paleogene lignite in the barmer basin, Rajasthan, India. *J. Asian Earth Sci.* 259, 105892. doi:10.1016/j.jseaes.2023. 105892
- Li, J., and Hu, S. (2017). History and future of the coal and coal chemical industry in China. *Resour. Conservation Recycl.* 124, 13–24. doi:10.1016/j.resconrec.2017.03.006
- Li, S., Tang, D., Pan, Z., and Xu, H. (2014). Influence and control of coal facies on physical properties of the coal reservoirs in Western Guizhou and eastern Yunnan, China. *Int. J. Oil, Gas Coal Technol.* 8 (2), 221–234. doi:10.1504/ijogct.2014. 064837
- Li, J., Yao, Z., Zhao, H., and Wang, Z. (2022). Gas hydrate stability zone in muri coalfield, Qinghai province, China. *Earth Environ. Sci. Trans. R. Soc. Edinb.* 113 (1), 7–12. doi:10.1017/s1755691021000311
- Lu, J., Shao, L., Yang, M., Zhou, K., Wheeley, J. R., Wang, H., et al. (2017). Depositional model for peat swamp and coal facies evolution using sedimentology, coal macerals, geochemistry and sequence stratigraphy. *J. Earth Sci.* 28, 1163–1177. doi:10.1007/s12583-016-0942-7
- Marchioni, D., and Kalkreuth, W. (1991). Coal facies interpretations based on lithotype and maceral variations in Lower Cretaceous (gates formation) coals of Western Canada. *Int. J. Coal Geol.* 18 (1-2), 125–162. doi:10.1016/0166-5162(91)90046-1
- McCabe, P. J. (1987). "Facies studies of coal and coal-bearing strata," $Geol.\ Soc.\ 32\ 1,\ 51-66.\ doi:10.1144/gsl.sp.1987.032.01.05$
- Moore, P. D. (1989). The ecology of peat-forming processes: a review. Int. J. Coal Geol. 12 (1-4), 89–103. doi:10.1016/0166-5162(89)90048-7

- Moore, T. A., and Shearer, J. C. (2003). Peat/coal type and depositional environment-are they related? *Int. J. Coal Geol.* 56 (3-4), 233–252. doi:10.1016/s0166-5162(03)00114-9
- Nath, M., and Kumar, A. (2022). A study of geochemical and petrographic characteristics of Eocene coal from bapung coalfield, east jaintia hills, Meghalaya, north East India. *Arabian J. Geosciences* 15 (8), 718. doi:10.1007/s12517-022-09950-2
- Pan, G., Xiao, Q., Lu, S., Den, J., Feng, Y., Zhang, K., et al. (2009). Subdivision of tectonic units in China. *Geol. China* 36 (1), 1–28.
- Pickel, W., Kus, J., Flores, D., Kalaitzidis, S., Christanis, K., Cardott, B. J., et al. (2017). Classification of liptinite-ICCP system 1994. *Int. J. Coal Geol.* 169, 40–61. doi:10.1016/j.coal.2016.11.004
- Ramsay, J. G., and Huber, M. I. (1987). *Modern structural geology*. San Diego, CA: Academic Press. 2, 309–700.
- Scott, A. C. (1989). Observations on the nature and origin of fusain. Int. J. Coal Geol. 12 (1-4), 443–475. doi:10.1016/0166-5162(89)90061-x
- Sen, S. (2016). Review on coal petrographic indices and models and their applicability in paleoenvironmental interpretation. *Geosciences J.* 20 (5), 719–729. doi:10.1007/s12303-015-0046-x
- Seyler, C. A. (1928). The dictyoxylon cortex of Lycopodiales as a constituent of coal. *Philosophical Trans. R. Soc. Lond. Ser. B, Contain. Pap. a Biol. Character* 216 (431-439), 353–362
- Shang, X., Shao, L., Zhang, W., Lv, J., Wang, W., Li, Y., et al. (2018). Sequence paleogeography and coal accumulation of the early-middle Jurassic in central qilian Mountain belt (muli basin), Qinghai province, northwestern China. *AAPG Bull.* 102 (9), 1739–1762. doi:10.1306/01081817063
- Shao, L. Y., Yang, Z. Y., Li, Y. H., Shang, X. X., Wang, W. C., Lv, J. G., et al. (2015). Lithofacies palaeogeography of the Middle Jurassic in the juhugeng gas hydrate potential area in muli, Qinghai province. *Geoscience* 29 (5), 1061–1072.
- Silva, M. B., and Kalkreuth, W. (2005). Petrological and geochemical characterization of candiota coal seams, Brazil-implication for coal facies interpretations and coal rank. *Int. J. Coal Geol.* 64 (3-4), 217–238. doi:10.1016/j.coal.2005.04.003
- Singh, A. K., and Kumar, A. (2017). Petro-chemical characterisation and depositional paleoenvironment of lignite deposits of nagaur, Western Rajasthan, India. *Environ. Earth Sci.* 76 (20), 692. doi:10.1007/s12665-017-7004-z
- Singh, A. K., and Kumar, A. (2020). Assessment of thermal maturity, source rock potential and paleodepositional environment of the Paleogene lignites in Barsingsar, Bikaner–nagaur basin, Western Rajasthan, India. *Nat. Resour. Res.* 29 (2), 1283–1305. doi:10.1007/s11053-019-09502-8
- Smith, G. C., and Cook, A. C. (1980). Coalification paths of exinite, vitrinite and inertite. Fuel 59 (9), 641-646. doi:10.1016/0016-2361(80)90127-1
- Suárez-Ruiz, I., and Jiménez, A. (2004). Coal facies studies in Spain. *Int. J. Coal Geol.* 58 (1-2), 31–39. doi:10.1016/j.coal.2003.06.002
- Taylor, G., Teichmüller, M., Davis, A., Diessel, C., Littke, R., and Robert, P. (1998). *Organic petrology*. Stuttgart, Berlin: Gebruder Bomntraeger.
- Wang, A., Cao, D., Li, J., Jiang, A., and Yang, C. (2017). A new discovery on the deformation behavior of shale gas reservoirs affecting pore morphology in the juhugeng coal mining area of Qinghai province, northwest China. *Acta Geol. Sinica-English Ed.* 91 (5), 1932–1933. doi:10.1111/1755-6724.13429
- Wang, A., Li, J., Wei, Y., Yang, C., Nie, J., and Cao, D. (2020). Gas migration for terrestrial gas hydrates in the juhugeng mining area of muli basin, qilian Mountains, northwest China. *Energy Explor. & Exploitation* 38 (4), 989–1013. doi:10.1177/0144598720910507
- Ward, C. R. (2016). Analysis, origin and significance of mineral matter in coal: an updated review. *Int. J. Coal Geol.* 165, 1–27. doi:10.1016/j.coal.2016.07.014
- Wen, H. J., Lu, J., Shang, L. J., Liu, T. J., Chen, J. F., Ju, Q., et al. (2006). A sequence stratigraphic discussion of the Jurassic coal measures in the juhugeng coalmine area in Qinghai province. *Coal Geol. China* 18 (5), 19–21.
- Wen, H. J., Shao, L. Y., Li, Y. H., Lu, J., Zhang, S. L., Wang, W. L., et al. (2011). Structure and stratigraphy of the juhugeng coal district at muli, tianjun County, Qinghai Province. *Geol. Bull. China* 30 (12), 1823–1828.
- Yang, D., Wang, Q., and Haikui, T. (2011). A study on Jurassic coalbearing rock series sedimentary facies in juhugeng mine area, Qinghai. *Coal Geol. China* 23, 15–17.
- Yang, Z. Y., Wang, W. C., Shao, L. Y., Liu, W. J., Lv, J. G., Li, Y. H., et al. (2015). Depositional environments of the Middle Jurassic in the sanlutian mining field of the juhugeng mining area in Qinghai province. *Geoscience* 29, 1073–1086.
- Yuan, J. (2018). The future of coal in China. Resour. Conservation Recycl. 129, 290-292. doi:10.1016/j.resconrec.2016.12.006
- Zhang, S., Tang, S., Tang, D., Pan, Z., and Yang, F. (2010). The characteristics of coal reservoir pores and coal facies in liulin district, hedong coal field of China. *Int. J. Coal Geol.* 81 (2), 117–127. doi:10.1016/j.coal.2009.11.007
- Zhao, L., Qin, Y., Cai, C., Xie, Y., Wang, G., Huang, B., et al. (2017). Control of coal facies to adsorption-desorption divergence of coals: a case from the xiqu drainage area, gujiao CBM block, north China. *Int. J. Coal Geol.* 171, 169–184. doi:10.1016/j.coal.2017.01.006